Composites Part B 288 (2025) 111866

Contents lists available at ScienceDirect

Composites Part B

journal homepage: www.elsevier.com/locate/composites

All-polymer syntactic foams: Linking large strain cyclic experiments to Quasilinear Viscoelastic modelling for materials characterisation

Sy-Ngoc Nguyen [a], Riccardo De Pascalis [b,*], Zeshan Yousaf [c,d], William J. Parnell [d]

[a] Department of Mechanical, Robotics and Energy Engineering, Dongguk University, Seoul 04620, Republic of Korea
[b] Dipartimento di Matematica e Fisica 'E. De Giorgi', Università del Salento, Via per Arnesano, 73100, Lecce, Italy
[c] Department of Materials, University of Manchester, Oxford Road, Manchester, M13 9PL, UK
[d] Department of Mathematics, University of Manchester, Oxford Road, Manchester, M13 9PL, UK

ARTICLE INFO

Keywords:
Particle-reinforcement
Polymer–matrix composites (PMCs)
Stress relaxation
Computational modelling
Mechanical testing

ABSTRACT

The time-dependent behaviour of polymeric composites is critical in a broad range of applications, including those in marine, aerospace, and automotive environments. In the present study, we assess the validity of the quasi-linear viscoelastic (QLV) model to fit the stress–strain behaviour of all-polymer syntactic foams under large cyclic compressional strain in a novel experimental configuration. These syntactic foams were manufactured by adding hollow polymer microspheres of various sizes and wall thicknesses into a polyurethane matrix. These materials are known for their relatively large initial stiffness, and strong recoverability after large strains. In the QLV model, several strain energy functions (SEFs) were employed, including neo-Hookean, Ogden type I, and type II. The bulk and shear moduli are presented in the form of a Prony series. By estimating these experimental data using optimisation, the natural viscoelastic material properties and coefficients associated with the SEF were determined. The influence of the microsphere filling fraction was also explored. We show that at the strain rate considered here of 0.013 s^{-1}, the compressible QLV model coupled with the Ogden-I SEF is capable of providing an excellent fit to experimental data. Critically, this fit can be achieved over a range of cycles via model optimisation to the first cyclic response only.

1. Introduction

Syntactic foams (SFs) are composite materials that are employed extensively in engineering structures in aerospace, marine, and automotive environments given their significant structural weight reduction coupled with relatively high stiffness [1–3]. Such composites are fabricated by placing spherical microscopic hollow particles into a matrix that is usually polymeric in nature and also known as *two-component polymer–matrix solid buoyancy materials* (PSBMs) [4]. The addition of hollow particles in the polymeric matrix makes the microstructure of SFs complex compared to the unfilled polymer–matrix with the emergence of three regions in the stress–strain curve of the SFs, namely the linear region, plateau region and finally, a densification region [5]. With the help of hollow *polymeric* microspheres, syntactic foams have the ability to undergo large deformation without failure and to achieve high energy absorption under compression [5,6]. Moreover, the (relatively) stiff shells give the syntactic foams an increased initial modulus (before deformation softens this somewhat) and increased strength to the pure matrix [7]. Glass microspheres have also been used extensively in syntactic foams [8]. Glass shells have the advantage of higher stiffness but the disadvantage that they fracture under sufficient load [9]. In addition, metal matrix syntactic foams composite have also been used for load bearing and lightweight applications. In metal syntactic foams, hollow or porous particles are incorporated within a metallic matrix alloy to provide the porosity of the material, and these foams exhibit high mechanical energy absorption, high specific stiffness, high strength-to-weight ratios, and tolerance to high temperatures and adverse environmental conditions [10–14].

A significant body of work has investigated the mechanical response of syntactic foams [6,15–22] with specific importance placed on their response under compression. It is not straightforward to predict mechanical properties theoretically since microspheres can take a variety of different forms and distributions in terms of their size distribution and also their physical, mechanical and chemical properties.

In terms of the constitutive response of the foam, the linear elastic region is predominantly associated with the stiffness provided by shells. Subsequently, as shells either fracture [9,23] or buckle [24,25], the plateau region is initiated, leading to larger strains and specifically to a potentially large increase in strain with only a small change in imposed

* Corresponding author.
E-mail addresses: riccardo.depascalis@unisalento.it (R. De Pascalis), William.J.Parnell@manchester.ac.uk (W.J. Parnell).

https://doi.org/10.1016/j.compositesb.2024.111866
Received 27 May 2024; Received in revised form 8 September 2024; Accepted 30 September 2024
Available online 11 October 2024

load. Finally, densification starts when the shells inside the syntactic foams begin to close up. This requires a large increase in stress to increase the strain by even a small amount. The nonlinear constitutive relationship can be described according to models of soft elastomers or hyperelastic materials [6,15,25–29].

In general, despite the matrix of syntactic foams being polymeric in many use cases, there is a lack of exploration of the time-dependent response of the viscoelastic behaviour of syntactic foams and, in particular, their relation to models. Although a small number of studies have investigated aspects of viscoelastic effects [30–34], there is a lack of investigation of the large strain cyclic viscoelastic response of polymeric syntactic foams. In this scenario, creep and relaxation play an important role. Creep refers to the gradual increase in strain under a constant load, which affects the foam's long-term deformation under sustained stress. Relaxation involves a decrease in stress under constant strain as the material adjusts over time. The interplay between creep and relaxation under cyclic loading reveals how the syntactic foams manage time-dependent deformations and stresses during cyclic loading. Understanding these effects helps in accurately modelling the material's viscoelastic behaviour [35–38], which is crucial for predicting its performance in real-world applications.

Numerous laws exist for modelling materials that behave in a linear viscoelastic manner, including the standard Boltzmann superposition integral forms [39–41]. The stress–strain response is assumed to be linear, with the time-dependent Prony relaxation modulus employed to good effect in many cases. Furthermore, with the help of transform tools, the computational work for linear viscoelasticity can be reduced by transformation into the Laplace domain and subsequent conversion for the results back in the time domain [42–45]. However, linear viscoelastic analysis is limited to analysing the response of composite polymeric materials by the hypothesis of small strains. This assumption becomes highly inaccurate for the viscoelastic response of elastomers due to their hyperelastic response, involving both large strain and constitutive nonlinearity. The strain is so large that it should be considered as a nonlinear viscoelastic medium. However, in the case of syntactic foams, the fillers add further complexity to the response, above and beyond standard viscoelastic polymers. A review of nonlinear models of viscoelasticity can be found in [46].

One of the most popular methods for viscoelastic modelling under large strain is Fung's quasi-linear viscoelasticity (QLV) [47–50]. This model is derived from the Boltzmann superposition principle but employs hyperelasticity and thereby accommodates large strain, as well as nonlinear constitutive behaviour via the incorporation of strain energy functions. The QLV model predicts that at any time, the stress is equal to the instantaneous elastic stress decreased by an amount that depends on the past history. It also assumes that the viscous relaxation rate is independent of the instantaneous local strain. A correspondence principle to obtain (when possible) QLV solutions from linear viscoelasticity is established in [51]. QLV has been widely used in simulations of a broad array of soft materials such as polymers, rubbers and biomaterials to name a few [52–60] and in investigating the influence of dissipation effects in pre-stressed soft phononic crystals [61,62], to study the existence of travelling waves [63] and in the modelling of membranes and beams [64–66]. However, it has not yet been understood if QLV is a valuable model in the context of polymeric syntactic foams.

The present study aims to assess the efficacy of QLV in modelling the cyclic axial stress–strain response of a class of all-polymer syntactic foams under large deformation. In particular, we consider foams with a polyurethane (PU) matrix and an Expancel-920 filler with 20% and 40% filling fractions (which we refer to as SF XX for the XX% filled foam). To our best knowledge [5,6], existing experimental data on the uniaxial cyclic compression of thermoplastic syntactic foams is only available when samples are not glued to the compression plates. This limits the ability to fit the model in the sense that it can only provide machine strain rather than actual sample strain, as the sample does not naturally return back to its original position during unloading after the initial loading; a gap opens up between the sample and the plate. To apply the actual strain and be consistent with the QLV theory employed for the fitting, rather than machine strain, in this work, we glued the samples on either side with the compression metal plates. This ensures that the 'memory' effect principle is satisfied according to the QLV model and avoids situations where the strain, in returning to zero after a loading/unloading cycle, leads the stress to vanish without accounting for the past history. This new approach for syntactic foams fulfilled the requirement of our model but also provided us with a chance to study the behaviour of thermoplastic syntactic foams with perfectly bonded boundaries; thus obtaining a new set of experimental data. In addition to allowing us to understand the fundamental behaviour of the foams and their constitutive response, the knowledge determined could also be helpful in applications where syntactic foams are glued on both sides, e.g. syntactic foams in sandwich structure applications [67].

Table 1
The assumed Poisson's ratio of the syntactic foam at volume fraction ϕ, under the Hencky model (1), with coefficients κ_i.

ϕ	$\nu_0 \approx \kappa_0$	κ_1	κ_2	κ_3
0%	0.49	–	–	–
20%	0.44	0.0218	−1.1894	−2.1454
40%	0.36	0.5421	0.6966	0.0710

In Section 2, we describe our experimental programme, detailing the configuration employed to assess the response of the foams in question. Section 3 introduces the Hencky function used in this study as a nonlinear Poisson's ratio. This establishes a nonlinear relation between lateral and longitudinal stretches. Section 4 covers the QLV model, describing the necessary constitutive approach and the hyperelastic modelling required (with neo-Hookean, Ogden-I, and Ogden-II SEFs) to set up the nonlinear viscoelastic response under large deformation. We fit this model to the experimental data via an optimisation method described in Section 5. This scheme minimises the root mean square error between the model and experimental data for each filling fraction scenario. We provide results in Section 6 and conclude, with suggestions for future work in Section 7.

2. Experimental configuration

2.1. Material

Polyurethane syntactic foams were manufactured by adding hollow thermoplastic microspheres into a polyurethane rubber matrix. The polyurethane was formulated from a blend of Polytetramethylene Ether Glycol (PTMEG) (Terathane 1000 supplied by INVISTA Textile (UK) Ltd), Trimethylolpropane (TMP) (Tokyo Chemical Industry), and cured with Methylene diphenyl diisocyanate (MDI) (Isonate M143 - Dow Chemicals). Fumed silica (Aerosil 200 – Evonik Inc.) was incorporated as a thixotropic additive. After mixing the hollow microspheres and polyurethane matrix, the mixture was degassed for air removal. Finally, the mixture was cured at 55°C [5]. Hollow microspheres were introduced into the matrix at a range of volume fractions of 20% and 40%. These and the pure polyurethane (0%), were investigated in detail in terms of their viscoelastic response under compressive load. The grade of hollow thermoplastic microspheres (HTMs) investigated here is 920 DE 80 d30 (Expancel grades supplied by Nouryon). Details of hollow microspheres are provided in Table 1. Scanning electron microscope (SEM) images of the HTMs and HTM syntactic foams (HTM SFs) at different magnifications are presented in Fig. 1. Measured and theoretically calculated densities of the resulting HTM SFs are presented in Fig. 2. Experimental density was measured by dividing the mass of the samples by its volume while theoretical density was measured by using the rule of mixture [68]. Values of both the measured and theoretical densities are in close agreement. The difference in the measured and theoretical densities for 20% and 40% volume fraction syntactic foams

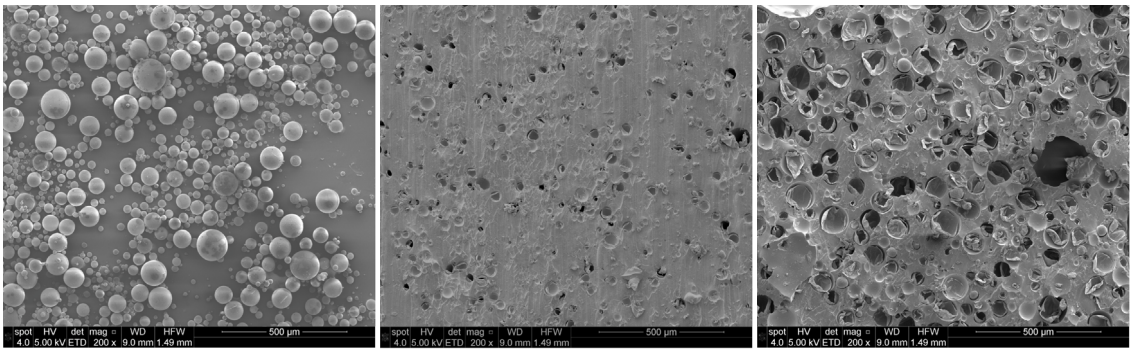

Fig. 1. SEM images of (a) Individual Expancel 920 microspheres and (b)-(c) Syntactic foam (20%–40% volume fraction), fabricated from a polyurethane matrix and Expancel-920 microspheres.

is 1.3% and 1.6%, respectively, showing only a small amount of voids entrapment/microsphere damage during processing. Additionally, a linear decrease in the densities of the syntactic foams with increasing microsphere volume fraction was observed. The decrease in density for SFs with 40% volume fraction microspheres was around 38% compared to neat polyurethane samples.

2.2. Mechanical testing

An Instron universal testing system with a load cell capacity of 100 kN was utilised to conduct uniaxial cyclic compression tests on the PU foam samples. The tests were conducted by following the ISO standard for vulcanised rubber (BS ISO 7743:2017 with method B). The test specimens were cut to a cylindrical shape. The diameter and height of the test specimens were 29 m and 12.5 mm, respectively. Specimens were bonded to metal plates with a diameter of 38 mm on the top and bottom surfaces using a thin layer of epoxy resin. The cross-head speed during the cyclic loading was maintained at 10 mm/min (thus a strain rate of $0.013\,s^{-1}$). Samples were compressed cyclically to 25% strain and left for a week to allow complete relaxation before further testing. After a week, samples were compressed to a strain of 50%. Five loading and unloading cycles were performed for both strain levels, and stress–time and stress–strain curves were recorded. The image of unfilled PU and SF 20% and 40% in unstrained and maximum compressed statements (50%) are shown in Fig. 3. From recorded data, to investigate the hyperelastic behaviours of SFs, the stress–strain response of unfilled PU and SF samples to 25% and 50% strain is shown in Fig. 4, where P here is the compressive stress, i.e. the negative of the nondimensional engineering stress under compressive loading (see Section 5 for its definition and scaling). Furthermore, to investigate the time-dependent behaviours of SFs, the stress–time response of these sample strains is shown in Fig. 5.

At the 25% strain level, the stress–strain and stress–time curves, shown in Figs. 4(a) and 5(a), respectively, of the unfilled samples presented a non-linear pattern that is normally associated with soft polymer materials. The time T represents the duration of each load cycle and is 1/5 of the total experimental time ($T/5$ is shown in the x-axes of Figs. 6–8(a–b)), which it is constant for all cycles, being the strain rate constant. Upon unloading the samples at the same strain rate as the loading cycle, an unloading curve with a slightly different path to the loading curve was recorded, forming a hysteresis loop describing the energy dissipation during cyclic loading. Additionally, given the strain-controlled deformation, the samples were left in a negative compressive stress state or tension during the deformation to zero strain. This negative stress state can be attributed to residual strain in the samples after the initial loading. A similar pattern was observed for successive loading and unloading curves for the unfilled specimen. For SF 20% and SF 40%, a different behaviour to the unfilled

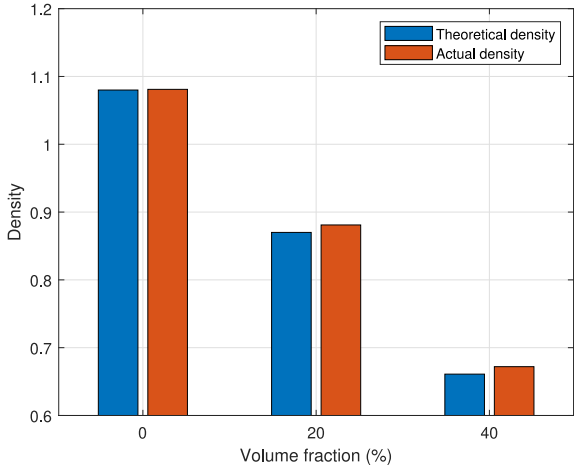

Fig. 2. Experimentally measured and theoretically predicted (using the arithmetic mean) effective mass density of the all-polymer syntactic foam samples, fabricated from a polyurethane matrix and Expancel-920 microspheres. The standard deviation for actual density is 0.0017 for unfilled and Expancel-920 40%, and 0.0023 for Expancel-920 20%. (For interpretation of the references to colour in this figure legend, the reader is referred to the web version of this article.)

PU samples was recorded. The SF samples showed an emergence of an initial linear region followed by a strong non-linear response. The initial linear region can be attributed to an increase in the initial stiffness of the SFs with the addition of the relatively stiff microspheres in the polymer–matrix. The successive four loading curves deviated from the pattern of the initial loading curve. A smaller force was required to compress the SFs in the four successive loading cycles compared to the first cycle. This smaller force can be attributed to the stress-softening after the first loading cycle [69]. Notably, the SFs exhibit stronger hysteresis during the unloading process compared to the unfilled PU samples, attributed to the phase lag between the applied stress and the resulting deformation. This phase lag arises from the time delay between stress application and the material's strain response, which is a fundamental characteristic of viscoelastic materials. Influenced by factors such as the material's relaxation behaviour, frequency of loading, and molecular structure, the phase lag reflects the material's ability to store and dissipate energy over time, shaping its viscoelastic response under cyclic loading conditions.

After conducting cyclic testing to 25% strain on the unfilled PU and SFs, the samples were left to fully relax for one week before proceeding to 50% compression cycles. The stress–strain and stress–time behaviours of the samples tested to 50% strain are presented in 4(b) and Fig. 5(b), respectively. Similar to the initial compression to

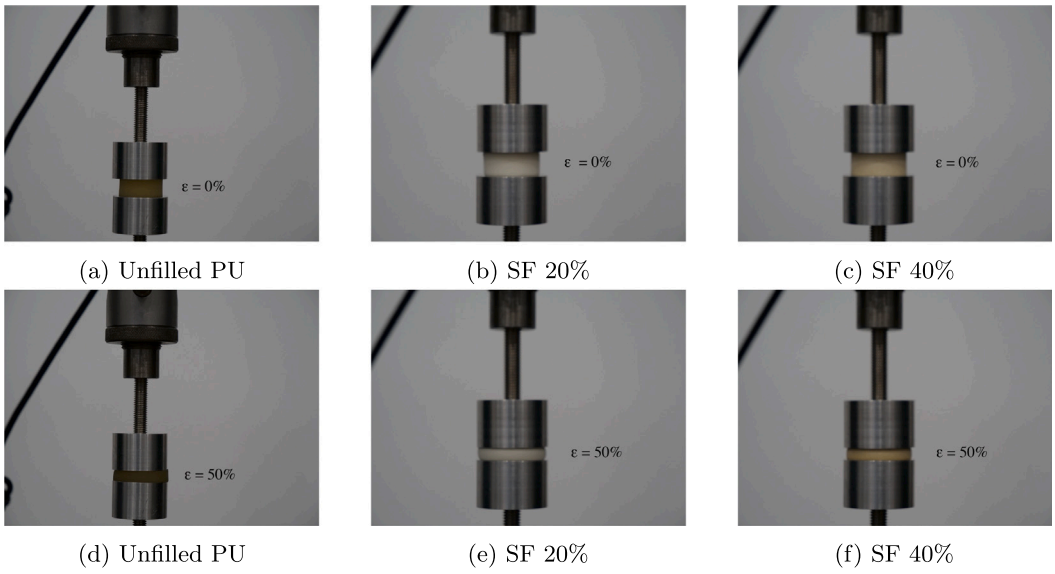

(a) Unfilled PU (b) SF 20% (c) SF 40%

(d) Unfilled PU (e) SF 20% (f) SF 40%

Fig. 3. Illustrating the experimental configuration for the compression cycles of unfilled polyurethane ((a),(d)) and a syntactic foam 20% volume fraction in ((b),(e)) and 40% volume fraction in ((c),(f)), fabricated from the same polyurethane matrix and Expancel-920 microspheres. Unstrained statement: (a) unfilled PU, (b) SF 20%, (c) SF 40%. 50% compressed statement: (d) unfilled PU, (e) SF 20%, (f) SF 40%.

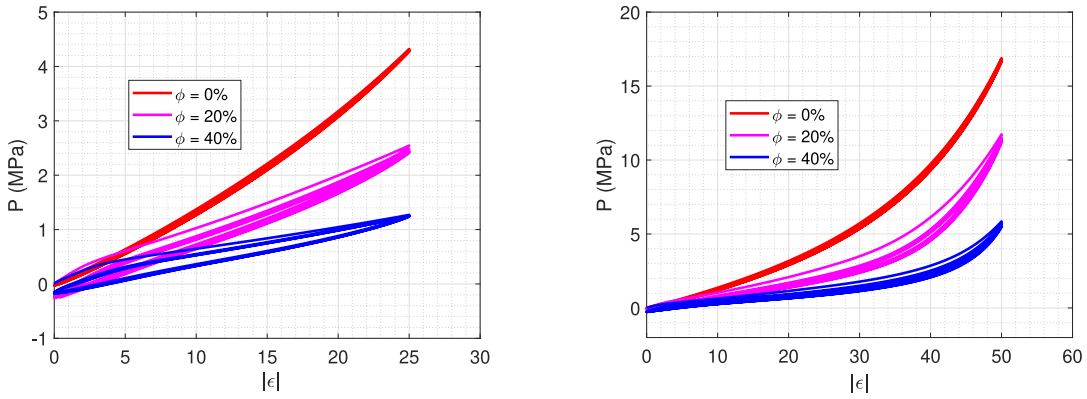

(a) Maximum strain 25% (b) Maximum strain 50%

Fig. 4. Experimentally measured stress–strain response of unfilled polyurethane and all-polymer syntactic foams at 20% and 40% volume fraction of microspheres, where P denotes the compressive stress. (For interpretation of the references to colour in this figure legend, the reader is referred to the web version of this article.)

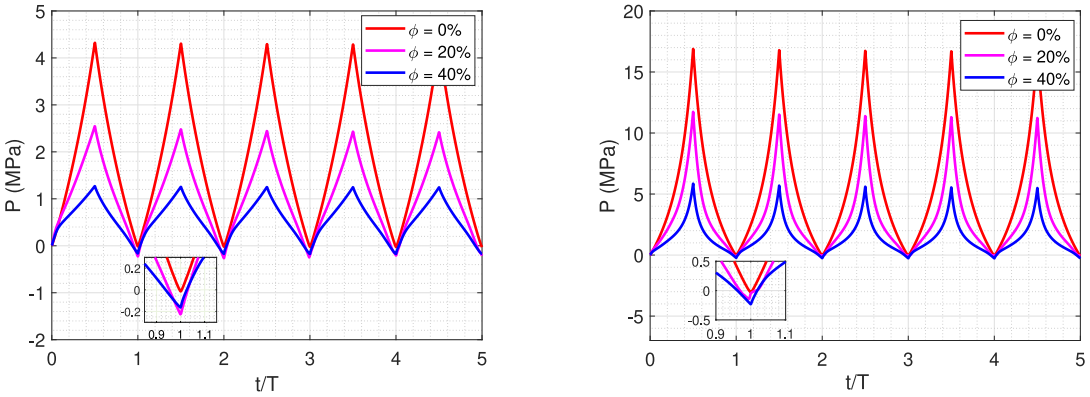

(a) Maximum strain 25% (b) Maximum strain 50%

Fig. 5. Experimentally measured stress–time response of unfilled polyurethane and all-polymer syntactic foams at 20% and 40% volume fraction of microspheres, where P denotes the compressive stress. Time is scaled on the single load cycle time T. (For interpretation of the references to colour in this figure legend, the reader is referred to the web version of this article.)

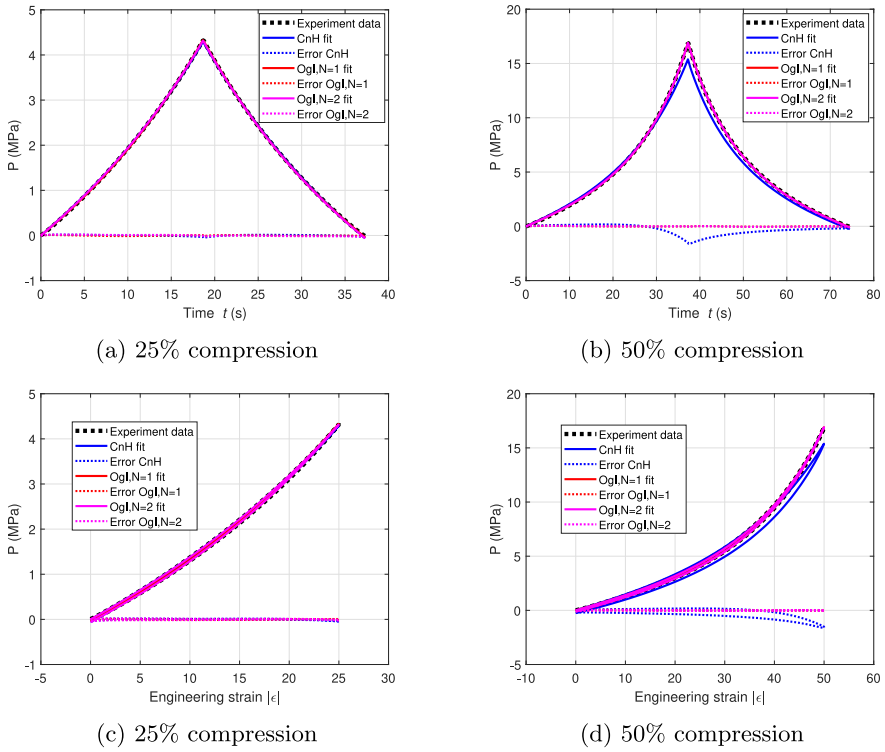

(a) 25% compression (b) 50% compression

(c) 25% compression (d) 50% compression

Fig. 6. Plots of the magnitude of the axial engineering stress P against time (a,b) and the associated stress–strain response (c,d) for the first cyclic compression of the unfilled PU. (For interpretation of the references to colour in this figure legend, the reader is referred to the web version of this article.)

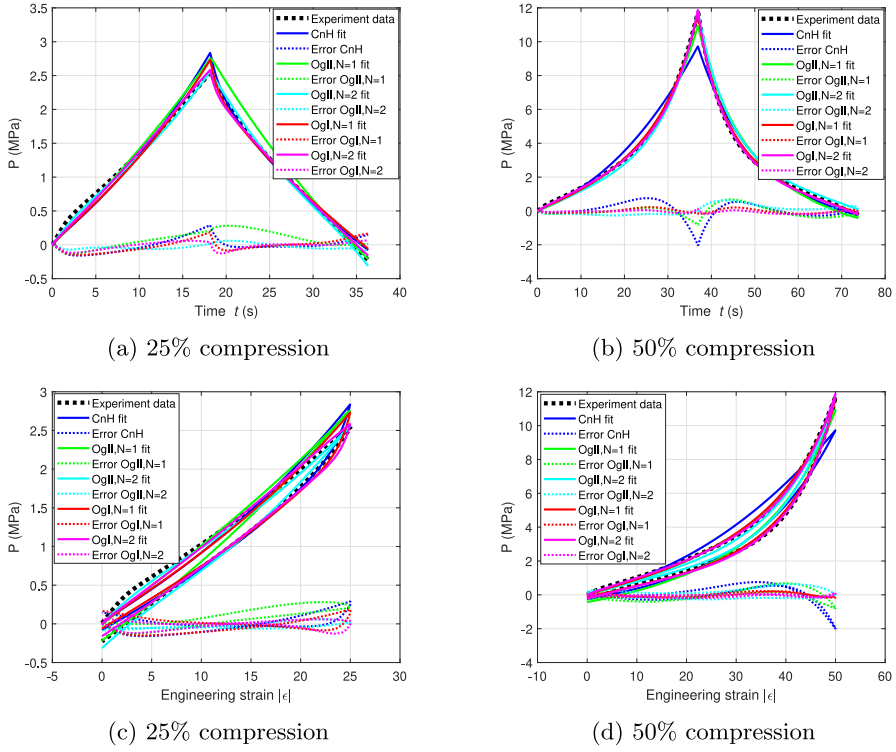

(a) 25% compression (b) 50% compression

(c) 25% compression (d) 50% compression

Fig. 7. Plots of the magnitude of the axial engineering stress P against time (a,b) and the associated stress–strain response (c,d) for the first cyclic compression of the syntactic foam with $\phi = 20\%$. (For interpretation of the references to colour in this figure legend, the reader is referred to the web version of this article.)

25% strain, the unfilled samples presented a non-linear behaviour for the cyclic compression to 50% strain. For SF compression to 50% strain, stress–strain curves again showed an initial linear region followed by a non-linear region, while hysteresis was evident on unloading cycles. These effects were especially strong for SF samples. The non-linear behaviour of the unfilled polyurethane and an initial linear region

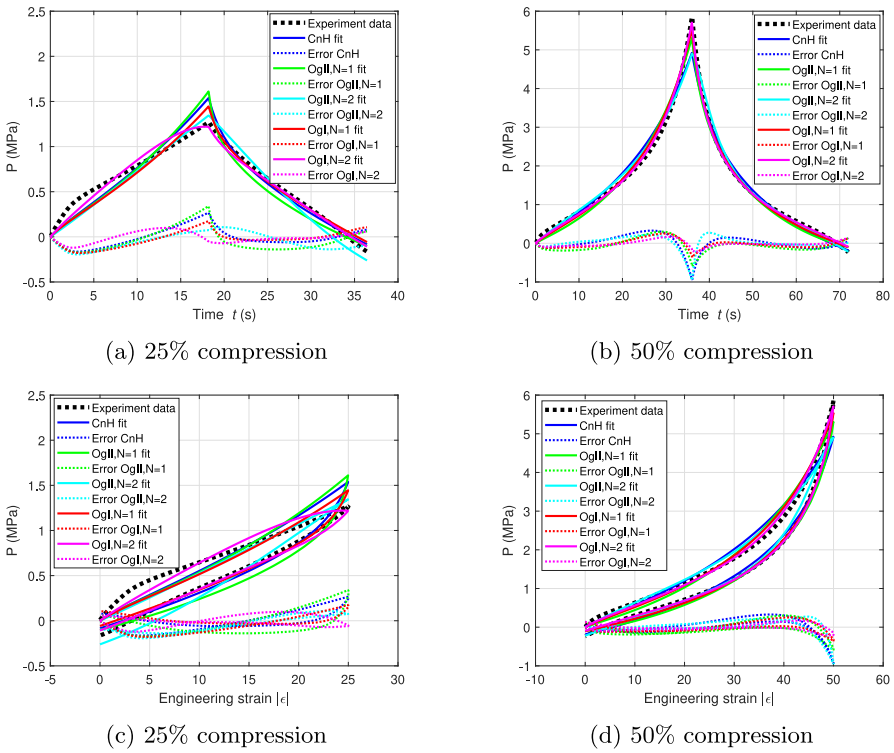

(a) 25% compression (b) 50% compression

(c) 25% compression (d) 50% compression

Fig. 8. Plots of the magnitude of the axial engineering stress P against time (a,b) and the associated stress–strain response (c,d) for the first cyclic compression of the syntactic foam with $\phi = 40\%$. (For interpretation of the references to colour in this figure legend, the reader is referred to the web version of this article.)

followed by a non-linear stress–strain response for SF samples on cyclic loading is in agreement with the already reported work on these types of materials [5].

3. Transverse-to-axial strain response and volume change

When subject to uniaxial compression unconstrained laterally the SF samples exhibit lateral strains. Upon loading, a barrelling effect was observed, which is also commonly reported for these types of materials even when they are not bonded [6]. This phenomenon adds complexity to uniaxial compression tests. We speculate that applying lateral confinement to the samples could prevent the barrelling effect. A separate study should be carried out to evaluate the impact of barrelling with and without lateral confinement. The uneven barrelling of the samples makes it challenging to measure the Poisson's ratio at a single point, as it changes along the length of the sample. Therefore, we measured the Poisson's ratio at multiple points along the sample and then averaged the results to minimise the impact of sample barrelling variation. For small deformations, the small strain *Poisson's ratio* ν_0 governs the ratio between the transverse and the longitudinal strain, with an upper bound $\nu_0 = 1/2$ for incompressible 'continuous' media, which do not allow volume changes. To describe this ratio under larger strains, and thus when nonlinear stress–strain constitutive laws must be employed, a more complex function of the strains has to be considered, namely the *Poisson function*. Among the most popular Poisson functions in nonlinear elasticity is the *Hencky* form [70]

$$\nu\left(\lambda_1\right) = -\frac{\log \lambda_2(\lambda_1)}{\log \lambda_1}, \tag{1}$$

where λ_1 denotes the axial (or longitudinal) stretch and λ_2 the radial (or transverse) stretch (defined as a function of λ_1). This Poisson function remains constant and equals $\nu = 1/2$ for incompressible materials (assuming $\lambda_2 = \lambda_1^{-1/2}$). It is worth noting that the small-strain Poisson's ratio ν_0 is recovered in (1) for transverse response $\lambda_2 \approx \lambda_1^{-\nu_0}$.

To fit the transverse stretches in the all-polymer SFs of interest here, the expression in (1) has been adopted in a recent work [6], which considers uniaxial loading up to compressive strains of 50%. It was shown that there is a strong dependence of λ_2 on the longitudinal stretch λ_1 for volume fractions $\phi > 10\%$. Furthermore, the choice $\lambda_2 \approx \lambda_1^{-\nu(\lambda_1)}$ with a third order polynomial

$$\nu\left(\lambda_1\right) \approx \kappa_3\left(\lambda_1 - 1\right)^3 + \kappa_2\left(\lambda_1 - 1\right)^2 + \kappa_1\left(\lambda_1 - 1\right) + \kappa_0, \tag{2}$$

was shown to describe well, qualitatively, the transverse response λ_2 as a function of the longitudinal imposed stretch λ_1. We note that this model of lateral response is not explicitly rate dependent, or rather, its rate dependence arises solely due to the rate dependence of λ_1 in the constitutive model.

Our chief focus here was the viscoelastic response of the medium in question, and therefore to reduce the number of unknown fitting parameters (and consequently the computational costs), we adopted the lateral stretch approximation (2), with coefficients κ_i $(i = 0, 1, 2, 3)$ as previously determined in [6], given that the same material was under consideration. We report this data in Table 1.

4. QLV for compressible materials under uniaxial compression

4.1. Constitutive equations

We focus on two main features of the mechanical response of syntactic foams under cyclic compression: large deformation and time-dependence. Although it is acknowledged that the quasilinear viscoelastic (QLV) model (also known as *Fung's quasi-linear constitutive model*) has some limitations, it has been successfully and widely employed for modelling the mechanical behaviour of soft materials ([56,59,60,71,72] to name a few among recent experimental studies). By considering the material behaviour as instantaneously elastic, the QLV model, which will be adopted here for model fitting, predicts that at any time, the total stress is modified by an amount depending on the past history through a strain-independent viscous relaxation tensor contracted with a potential (described shortly), and according to a Boltzmann superposition principle. This formulation was given a modern interpretation

in [48,73], and the associated constitutive law can be written for the most general isotropic compressible materials as:

$$\boldsymbol{\Pi}(t) = \int_{-\infty}^{t} \mathcal{D}(t-s)\,\frac{\partial}{\partial s}\boldsymbol{\Pi}^{\mathrm{e}}_{\mathrm{D}}(s)\,\mathrm{d}s + \int_{-\infty}^{t} \mathcal{H}(t-s)\,\frac{\partial}{\partial s}\boldsymbol{\Pi}^{\mathrm{e}}_{\mathrm{H}}(s)\,\mathrm{d}s, \tag{3}$$

where $\boldsymbol{\Pi}$ is the second Piola–Kirchhoff stress, t is time, and the scalar functions $\mathcal{D}$ and $\mathcal{H}$ are time-dependent reduced-relaxation functions associated with the deviatoric and hydrostatic responses, respectively (satisfying $\mathcal{D}(0) = \mathcal{H}(0) = 1$). It is worth noticing that by integrating (3) by parts, and assuming that the deformation commences at $t = 0$ (hence no deformation at $t = 0$ and $\boldsymbol{\Pi}^{\mathrm{e}}(0) = \mathbf{0}$), yields

$$\boldsymbol{\Pi}(t) = \boldsymbol{\Pi}^{\mathrm{e}}(t) + \int_{0}^{t} \mathcal{D}'(t-s)\,\boldsymbol{\Pi}^{\mathrm{e}}_{\mathrm{D}}(s)\,\mathrm{d}s + \int_{0}^{t} \mathcal{H}'(t-s)\,\boldsymbol{\Pi}^{\mathrm{e}}_{\mathrm{H}}(s)\,\mathrm{d}s, \tag{4}$$

where the $'$ denotes differentiation with respect to the argument of the function and the equivalence $\boldsymbol{\Pi}^{\mathrm{e}} = \boldsymbol{\Pi}^{\mathrm{e}}_{\mathrm{D}} + \boldsymbol{\Pi}^{\mathrm{e}}_{\mathrm{H}}$ has been used. The expression in (4) states that the viscoelastic stress is equal to the instantaneous elastic stress response (first term) decreased by an amount depending on the past history (terms under the integral). In particular, the integral terms are given by superposing linearly (*superposition principle* or *Boltzmann's principle*) the effects of a past amount of stress according to a fading principle governed by respective relaxation functions $\mathcal{D}, \mathcal{H}$. For further details, we refer to [48], where a careful derivation is made by starting from the simplest linearised version of viscoelasticity. We consider relaxation functions to be classical and frequently employed functions expressed in the form of the Prony series, as follows:

$$\mathcal{D}(t) = \frac{\mu_\infty}{\mu} + \sum_{i=1}^{p} \frac{\mu_i}{\mu} e^{-t/\tau_i^{\mathrm{D}}}, \qquad \mathcal{H}(t) = \frac{\kappa_\infty}{\kappa} + \sum_{i=1}^{p} \frac{\kappa_i}{\kappa} e^{-t/\tau_i^{\mathrm{H}}}, \tag{5}$$

satisfying the constraints

$$\frac{\mu_\infty}{\mu} + \sum_{i=1}^{p} \frac{\mu_i}{\mu} = 1, \qquad \frac{\kappa_\infty}{\kappa} + \sum_{i=1}^{p} \frac{\kappa_i}{\kappa} = 1, \tag{6}$$

where (for a given integer $p > 0$ and for $i = 1, \ldots, p$) $\tau_i^{\mathrm{D}}, \tau_i^{\mathrm{H}}$ are the characteristic relaxation times, $\mu, \mu_\infty, \kappa, \kappa_\infty$ are the infinitesimal and long-time infinitesimal shear and bulk modulus, respectively and finally μ_i, κ_i are coefficients.

Here, we recall the relationship between the second Piola–Kirchhoff stress and alternative stress measures. Define the deformation gradient $\mathbf{F}$, which, for the deformation under consideration here, can be written in a diagonal form in terms of the principal stretches as $\mathbf{F} = \mathrm{diag}\left(\lambda_1, \lambda_2, \lambda_3\right)$. The engineering stress is defined as $\mathbf{P} = \mathbf{F}\boldsymbol{\Pi}$ and the Cauchy stress is $\mathbf{T} = \frac{1}{J}\mathbf{F}\boldsymbol{\Pi}\mathbf{F}^{\mathrm{T}}$, where the superscript 'T' denotes the transpose.

4.2. Hyperelastic modelling for large-deformation in compression

Materials capable of large elastic deformations can be associated with a potential W, also known as the strain energy function (SEF). Under the assumption of isotropy, this can be written as a symmetric function of the principal stretches of the deformation, i.e. $W = W(\lambda_1, \lambda_2, \lambda_3)$ [74]. Recall that in our experiments and associated model, we assume $\lambda_2 = \lambda_3$ due to the assumption of ideal uniaxial compression.

For compressible hyperelastic materials, the standard approach is to decompose the SEF into isochoric and volumetric parts, as follows

$$W = W_{\mathrm{iso}}\left(\lambda_1, \lambda_2, \lambda_3\right) + W_{\mathrm{vol}}(J), \tag{7}$$

where $J = \det\mathbf{F} = \lambda_1\lambda_2^2$ (since $\lambda_2 = \lambda_3$) is the volume ratio of the model during compression, with $J = 1$ describing constrained incompressible materials. In Eqs. (3)–(4), $\boldsymbol{\Pi}^{\mathrm{e}}_{\mathrm{D}}$ and $\boldsymbol{\Pi}^{\mathrm{e}}_{\mathrm{H}}$ correspond to the second Piola–Kirchhoff stress of the deviatoric and hydrostatic Cauchy stress components, respectively whose diagonal non-vanishing components $\Pi^{\mathrm{e}}_{\mathrm{D}i}, \Pi^{\mathrm{e}}_{\mathrm{H}i}$ $(i = 1, 2, 3)$ are as follows:

$$\Pi^{\mathrm{e}}_{\mathrm{D}i} = \frac{W_i}{\lambda_i} - \frac{1}{3\lambda_i^2}\sum_{j=1}^{3}\lambda_j W_j, \qquad \Pi^{\mathrm{e}}_{\mathrm{H}i} = \frac{1}{3\lambda_i^2}\sum_{j=1}^{3}\lambda_j W_j, \tag{8}$$

where $W_j = \partial W/\partial\lambda_j$. We refer the reader to [48] for details of the derivation.

To attempt to fit the compressional stress–strain cyclic tests of the syntactic foams under investigation, there are a plethora of SEFs from which to choose. The QLV theory extends the nonlinear elastic theory to include the dissipative effects. In our assumptions, the instantaneous elastic stress is written in terms of W (hyperelasticity), while the viscoelastic stress is a convolution between the elastic stress and the reduced relaxation function tensor. This means that the viscoelastic stress obtained from the hyperelastic stress is decreased by an amount depending on the past history by considering a fading memory principle through the scalar functions $\mathcal{D}, \mathcal{H}$. Thus, the SEF includes instantaneous elastic moduli only while other (longer-time) elastic moduli and relaxation times are included in $\mathcal{D}, \mathcal{H}$. We refer to Section 4(a-b) of [61] for a better comprehension of the equivalence, in the quasi-static regime, between the QLV and hyperelastic theory. In particular, in the paper [61], a simple uniaxial incompressible deformation has been analysed with $p = 1$ in (5), and creep and relaxation tests have been carried which show clearly how the long time limit of viscoelastic stress is equivalent to an elastic theory which instead of instantaneous elastic model employ long-time elastic moduli.

We therefore consider those SEFs employed most extensively in the context of the elastic response of elastomeric and syntactic foams [6, 74–76], which are compressible neo-Hookean (CnH), Ogden type-I (OgI) and Ogden type-II (OgII) strain energy models. The adopted SEF models are listed in the following, where the integer $N > 0$ is considered as the order of the model.

Compressible neo-Hookean (CnH)

$$W = C_{10}\left(\bar{\lambda}_1^2 + \bar{\lambda}_2^2 + \bar{\lambda}_3^2 - 3\right) + \frac{1}{D_1}(J-1)^2, \tag{9}$$

where C_{10} and D_1 are scalar parameters which relate to small-strain material constants in the following manner:

$$2C_{10} = \mu, \qquad \frac{2}{D_1} = \kappa. \tag{10}$$

Compressible Ogden type I (OgI)

$$W = \sum_{j=1}^{N}\left\{\frac{2\eta_j}{\alpha_j^2}\left(\bar{\lambda}_1^{\alpha_j} + \bar{\lambda}_2^{\alpha_j} + \bar{\lambda}_3^{\alpha_j} - 3\right) + \frac{1}{D_j}(J-1)^{2j}\right\}, \tag{11}$$

where $\eta_j > 0$, α_j and D_j $(j = 1, \ldots, N)$ are real-valued constants which are related to small-strain constants in the following manner:

$$\sum_{j=1}^{N}\eta_j = \mu, \qquad \frac{2}{D_1} = \kappa. \tag{12}$$

Compressible Ogden type II (OgII)

$$W = \sum_{j=1}^{N}\frac{2\eta_j}{\alpha_j^2}\left\{\lambda_1^{\alpha_j} + \lambda_2^{\alpha_j} + \lambda_3^{\alpha_j} - 3 + \frac{1}{\beta_j}\left(J^{-\alpha_j\beta_j} - 1\right)\right\}, \tag{13}$$

where α_j, β_j and $\eta_j > 0$ $(j = 1, \ldots, N)$ are scalar parameters which relate to small-strain material constants in the following manner:

$$\sum_{j=1}^{N}\eta_j = \mu, \qquad \sum_{j=1}^{N}2\eta_j\left(\beta_j + \frac{1}{3}\right) = \kappa. \tag{14}$$

It is worth noticing that the above SEFs are the same employed in [6] where hyperelastic models have been used to fit the loading curves. Consistently, we here fit the experimental data by extending hyperelasticity to the more general QLV theory, which also accounts for the dissipative effects shown by the loading/unloading curves considered in the analysis. This and historical reasons have led us to present the SEF models by using both the principal stretch λ_i and their modified

version. Indeed, CnH and OgI in (9) and (11), respectively, are written in terms of the so-called *reduced* principal stretches

$$\bar{\lambda}_i = J^{-1/3}\lambda_i \tag{15}$$

for $i = 1,2,3$, which allows the deformation to be decomposed in its dilatational and distortional parts [77]. So that, for $(j = 1,\dots,N)$ the coefficients C_{10}, η_j, α_j, describe the shear behaviour of the material while D_j the compressibility [78]. We precise that with the terminology *Ogden type model* we refer to them according to the seminal work of Ogden [79] who, to simplify the associated mathematical analysis involved in describing rubberlike experiments, considered the incompressible SEF written as a linear combination of the strain invariants $\Phi(\alpha) = \left(\lambda_1^\alpha + \lambda_2^\alpha + \lambda_3^\alpha - 3\right)/\alpha$ where α is a real number. Both models have been implemented in ABAQUS software, and in particular, OgII [75] is based on the proposed model given by Hill [80,81].

5. Optimisation for QLV model fitting

We are interested primarily in the axial engineering stress component $P_1 = \lambda_1 \Pi_1$ and its relation to axial strain. This stress can be obtained by employing one of the SEFs given in (9), (11) and (13), the relations (8), and the constitutive law (3). To simplify notation, we drop subscripts and, given that we are principally interested in compressive stress, we write $P = -P_1$. We denote the longitudinal engineering strain by $\epsilon = \lambda_1 - 1$. In order to attempt to characterise the mechanical properties and time-dependent relaxation functions incorporated into the QLV model, we optimise the fit between the model and the experimental data. To do this, we adopt a parameter-fitting procedure based on the following optimisation problem.

We wish to minimise the root mean squared error (RMSE) defined as

$$\text{RMSE} = \sqrt{\sum_{i=1}^{M} \frac{(x_i - \hat{x}_i)^2}{M}}, \tag{16}$$

where here $\hat{x}_i$ are the predicted values from the model, x_i are the observed values from experimental data and M is the number of observations. This is subject to the relations

$$\mu_\infty + \sum_{i=1}^{p} \mu_i = \mu \qquad \kappa_\infty + \sum_{i=1}^{p} \kappa_i = \kappa \tag{17}$$

$$\text{and subject to}: \begin{cases} 2C_{10} = \mu, \ {}^2/_{D_1} = \kappa, & \text{(CnH)} \\ \sum_{j=1}^{N} \eta_j = \mu, \ {}^2/_{D_1} = \kappa, & \text{(OgI)} \\ \sum_{j=1}^{N} \eta_j = \mu, \ \sum_{j=1}^{N} 2\eta_j \left(\beta_j + {}^1/_3\right) = \kappa, & \text{(OgII)} \end{cases} \tag{18}$$

and furthermore we impose $\eta_j > 0$ to ensure a more stable optimisation process [82]. Since it transpires that the output results of all process cycles are found to be very similar to those of the first cyclic duration, to reduce computational costs, only the response of the first cyclic duration is considered, while the subsequent cyclic durations with similar responses are disregarded.

Due to its efficiency, robustness, and scalability, the Surrogate Optimisation Algorithm (SOA) has been employed to determine the final material coefficients of all syntactic foams for a given SEF. By using a surrogate model to estimate the objective function of an optimisation problem, the algorithm can significantly decrease the computational costs of evaluating the objective function (making it particularly efficient for problems with computationally expensive objective functions) [83,84]. Furthermore, the SOA can handle noisy or complex objective functions. The surrogate model can help the algorithm to smooth out the noise and identify the global optimum. Additionally, the SOA is highly scalable and can handle high-dimensional and complex optimisation problems more effectively by reducing the search space and exploring it more intelligently, making it a potent tool for our optimisation problems.

6. Results & discussion

To assess the model's fit to the experimental data, we conducted several investigations, which are discussed below. The root mean square error (RMSE) (which, through the whole paper, we write in non-dimensional form by scaling it by 1 MPa) values for all investigations are summarised in Appendix B. We refer to these values as a measure for comparing the fitting of the following sections.

6.1. Comparison of models to experimental data

The efficacy of the QLV model is here analysed by employing it in association with compressible neo-Hookean SEF and Ogden type-I and type-II SEFs with order $N = 1,2$, and we refer to them by the abbreviations as in Section 4.2. Results obtained by the SOA are compared to experimental data in Figs. 6–8 for filling fractions 0% (a case that we also refer to as *unfilled* or *unfilled PU*), 20%, and 40%, respectively. Plots show the evolution of the axial engineering stress versus time in (a) and (b) and the stress–strain curves for 25% and 50% compression strain in (c) and (d), respectively. The dotted curves show the error (as a difference) between those from the model fit and the experiment. It is worth noting that for unfilled polyurethane (see Fig. 6), the material is not foam, and in that case, all fitted models exhibit reasonable accuracy, as we now discuss. It is worth noting that the blue and red curves in Fig. 6 are not very visible as they almost overlap with the OgI (N = 2) model.

For the unfilled PU case, the CnH model exhibits greater error when subjected to a 50% strain test compared to the 25% strain case, indicating its limited effectiveness under higher strain conditions. On the other hand, the OgI model with $N = 1$ proves to be more robust, maintaining a low error even at 50% strain, demonstrating its effectiveness in handling larger deformations. However, due to potential numerical instabilities associated with almost-incompressible syntactic foams, the OgII model for unfilled polyurethane was excluded from the analysis.

The increase in volume fraction and subsequent increase in the fraction of hollow microspheres gives rise to stronger microstructure evolution and leads to the potential for a larger discrepancy between model and experimental data, especially at large strains. There is strong evidence to suggest that hollow microspheres buckle under large strain compression. Such instabilities soften the foam locally with a prominent change in overall macroscopic mechanical response and convexity of the stress–strain curve [5,6,85]. It is challenging to model such a response via a macroscopic model that does not explicitly include complex microstructure behaviour. Only a small number of studies have considered microstructural models of syntactic foams at large strain (see, e.g. [27,86] which considered the case of compressive hydrostatic loading) but without viscoelastic effects. Here, we assess the ability of large-strain QLV models to incorporate the time-dependent, large-strain response for 20% and 40% volume fractions.

Let us first consider the case of the syntactic foam with a filling fraction of $\phi = 20\%$. Referring to Fig. 7, we note that the CnH model, the simplest of the SEFs considered, continues to exhibit the highest error, which is to be expected given its simplicity. In contrast, the OgII model demonstrates better performance, particularly when using higher-order terms ($N = 1$ and $N = 2$), which enhance its accuracy under strain. Overall, the OgI model achieves the best fitting performance, indicating that incorporating reduced stretches $\bar{\lambda}_i$ effectively improves the model's accuracy. However, despite the improved performance of the more complex SEF models, all of them struggle to accurately predict the peak stress relative to the maximum strain.

A syntactic foam with a filling fraction of $\phi = 40\%$ increases further the complexity of its microstructure, and consequently, the response under compression becomes more challenging to model. The peak of the stress at maximum deformation or the change of convexity of the

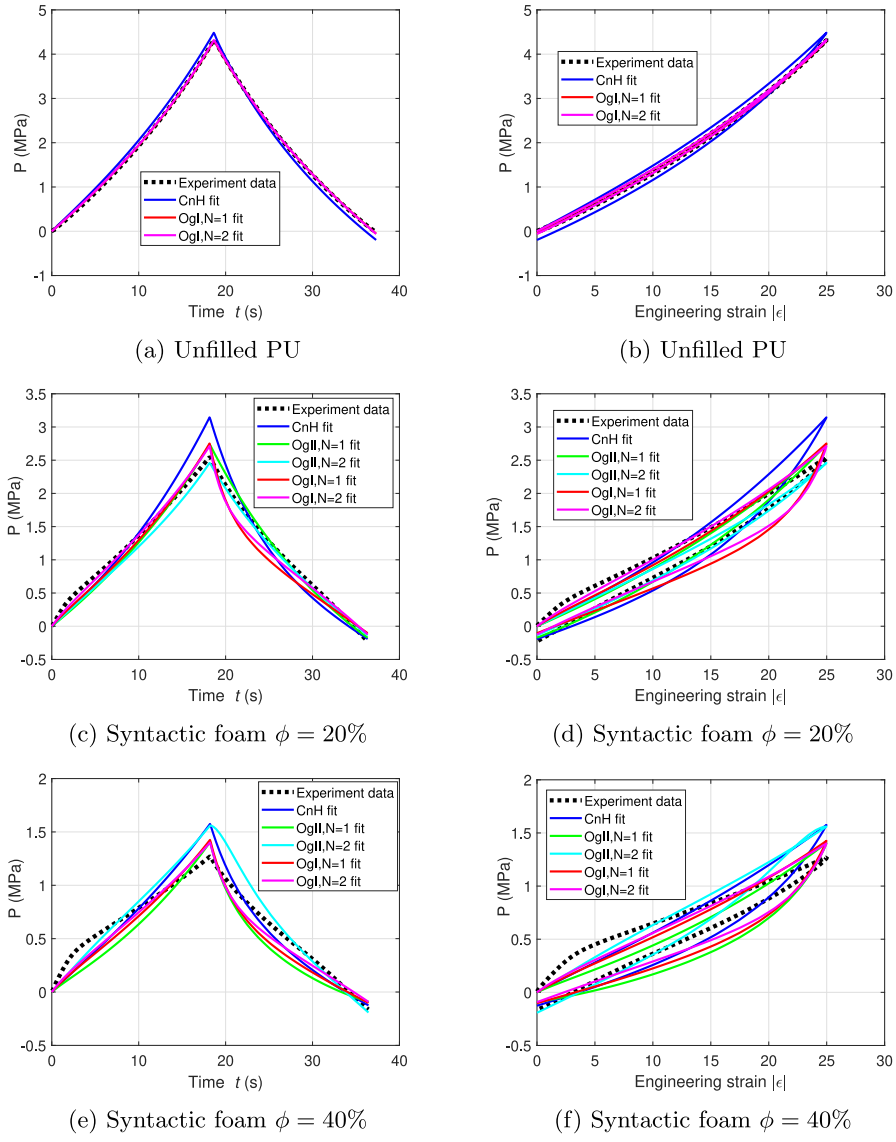

Fig. 9. Testing of the 50% fitted model on the lower strain 25% experimental data of (a,b) unfilled PU, (c,d) syntactic foams $\phi = 20\%$ and (e,f) syntactic foams $\phi = 40\%$. (For interpretation of the references to colour in this figure legend, the reader is referred to the web version of this article.)

stress for increasing strains is unlikely to be predictable. However, as we now show, a reasonable overall macroscopic fitting can be achieved.

As shown in Fig. 8, particularly for a 50% strain compression (plots (b,d)), the CnH model continues to exhibit the highest error, as expected given its simpler structure. The OgII model demonstrates improved performance, with better accuracy achieved for both $N = 1$ and $N = 2$. Once again, the OgI model performs the best, indicating that it is the most effective in capturing material behaviour under compression. Generally, increasing N can enhance fitting accuracy, though it comes with the trade-off of higher computational costs and the potential risk of over-fitting. In our analysis, the number of function evaluations was capped at 3000 to maintain computational efficiency.

It is of paramount importance to carefully choose the appropriate strain energy function and the optimal number of truncation order values, as this selection significantly influences the accuracy attained in fitting the mathematical model to the experimental data.

6.2. Accuracy of the models across strain levels

To assess the reliability of the fitted models, we attempted to describe experimental data corresponding to the compression up to 50% by using the fitted model obtained by experimental data with lower compression, i.e. up to 25% and vice-versa for the three cases under consideration: unfilled, 20% and 40% filling fractions.

6.2.1. Testing the 50% fitted model for the lower strain 25% experiment data

In Fig. 9, the results for unfilled PU and syntactic foams with 20% and 40% filling fractions are presented. All models fitted for higher strain (50%) remain stable when applied to lower strain (25%), though they exhibit slightly larger errors compared to models fitted specifically for 25% strain. The OgI and OgII models demonstrate high accuracy, underscoring their effectiveness, while the CnH model also performs well but with a slightly higher error.

6.2.2. Testing the 25% fitted model for the 50% experiment data

Understanding how well models trained in lower strain data handle higher strain conditions is important to assess their overall performance and reliability, especially for syntactic foam with complicated behaviour. In Fig. 10(a,b), the results for $\phi = 0\%$ show that all fitted models are stable due to the simplicity of the mechanical response of unfilled PU. The OgI model with $N = 1$ achieves the highest accuracy,

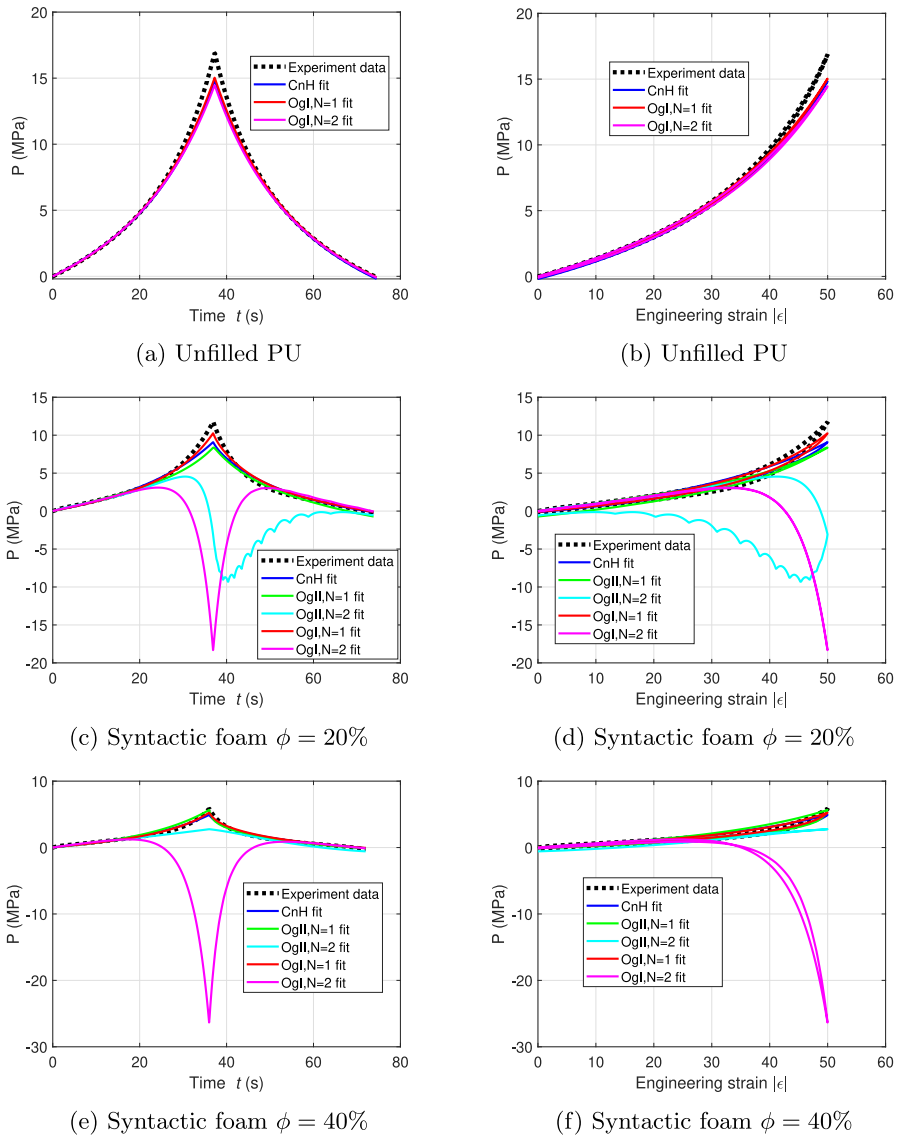

Fig. 10. Testing of the 25% fitted model on the higher strain 50% experimental data of (a,b) unfilled PU (c,d) syntactic foams $\phi = 20\%$ and (e,f) syntactic foams $\phi = 40\%$. OgI and OgII models are seen as unstable at higher strains beyond the regime of fitting. (For interpretation of the references to colour in this figure legend, the reader is referred to the web version of this article.)

while the CnH model also performs well. However, the OgI model with $N = 2$ shows reduced accuracy, suggesting that increasing the number of coefficients in the strain energy function may only improve fitting locally and may not sustain performance when using a larger number of coefficients.

In Fig. 10(c, d) and (e,f), the stress–strain response results for syntactic foams with a filling fraction of 20% and 40% are shown respectively. As previously observed, modelling the mechanical behaviour of these foams is more challenging when using a fit model of the lower strain to fit the higher strain. The CnH and OgII models with $N = 1$ demonstrate good accuracy, but again, the OgI model with $N = 1$ shows the highest accuracy.

Unfortunately, for both types of syntactic foams (20% and 40%), increasing the order to $N = 2$ leads to numerical instability in both OgI and OgII with an associated loss of accuracy in describing the mechanical response at larger strains (50%). This demonstrates that while having a larger number of parameters can enhance the fitting from one perspective, it can result in decreased control in fitting experimental data if the model was previously fitted on a subset of data, in addition to increased computational costs.

Overall, the analysis suggests that the hyperelastic models fitted to higher strain data can be used consistently and reliably to predict the behaviour at lower strains. Using lower strain data to predict deformation at higher strains is not reliable generally, although some models are better than others, noting that OgI and OgII are unstable numerically.

6.3. Accuracy of the model fit for the subsequent cyclic compression

To assess the reliability of our fitted models for subsequent cyclic loading, we projected stress versus time and stress–strain responses for all five cycles and compared them to experimental data for two sets of data: unfilled PU and 40% of filling fractions syntactic foam. The OgI model with $N = 2$ achieved the highest accuracy, with RMSE values of 0.1105 and 0.2357 for unfilled PU and syntactic foam 40%, respectively, while the CnH model remained stable but less accurate, with RMSE values of 0.5065 and 0.3094 for unfilled PU and syntactic foam 40%, respectively.

As shown in Fig. 11, CnH and OgI models are stable and accurate in subsequent cyclic periods for unfilled PU and syntactic foams 40%

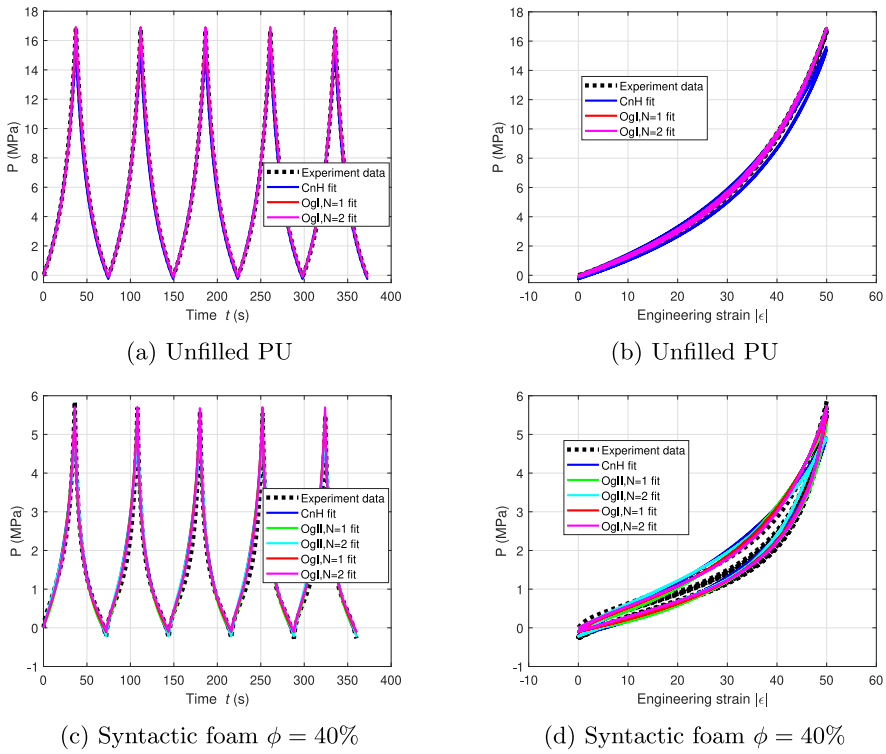

(a) Unfilled PU (b) Unfilled PU

(c) Syntactic foam $\phi = 40\%$ (d) Syntactic foam $\phi = 40\%$

Fig. 11. Testing of the fit models with 50% strain for the next following cyclic compression for unfilled PU (a,b) and 40% syntactic foam (c,d). (For interpretation of the references to colour in this figure legend, the reader is referred to the web version of this article.)

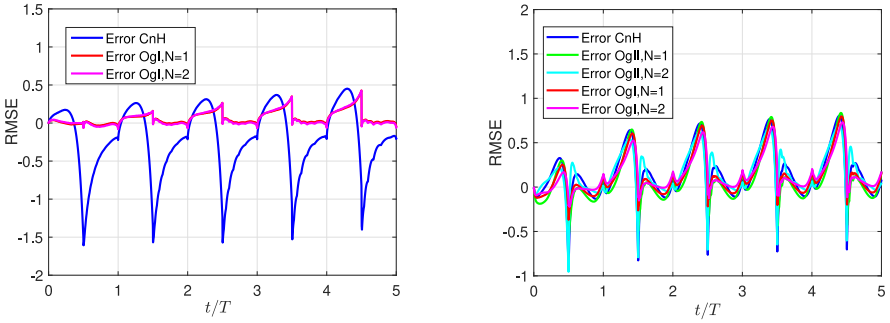

(a) Unfilled PU (b) Syntactic foam $\phi = 40\%$

Fig. 12. The error of fit models with 50% strain for the following compression cycles. (For interpretation of the references to colour in this figure legend, the reader is referred to the web version of this article.)

at up 50% of strain. The respective error of fit models compared to experiments is displayed in Fig. 12. There are two notable issues. Firstly, for syntactic foams at 40% filling fraction, as emphasised in Fig. 13, there is a reduction in the maximum stress during the following cycles of compression related to plastic deformation. This is hypothesised as being due to the microsphere hollow particles being unable, after buckling at a certain compression, to recover back and these effects are not included in our study. Indeed, this phenomenon cannot occur in unfilled PU. Secondly, accurately modelling stress from the second cyclic period is challenging because we used the same compression strain energy function for both the loading and unloading processes. Separating the compression strain energy function into two functions, one for loading and another for unloading, would improve accuracy. However, this would also significantly increase the formulation and computational costs.

6.4. Influence of filling fraction on the Young's modulus

The instantaneous elastic modulus Y is obtained from the optimisation process. Initially, we set up min and max values for Young modulus, and the optimisation code will find the appropriate Y value for the best fit between the mathematical model and the experimental data. Fig. 14 shows the estimated values of Y for compression up to 25% in (a) and 50% in (b) for the respective volume fractions and model fitting. The overall magnitude of the estimations is consistent in all cases, relative to unfilled and SFs and also by comparing the 25% and 50% of a compression test. A slight discrepancy from the mean value is given for 40% SF up 50% of the strains by the OgII model (where $N = 1$ gives a lower modulus than $N = 2$).

It is worth noting that the estimated instantaneous Young modulus, obtained via this nonlinear fitting procedure, decreases with an increasing filler volume fraction. This is consistent with the trend in an analogous fitting procedure associated with nonlinear elastic models [6]. Note that this is somewhat in contrast to the experimentally

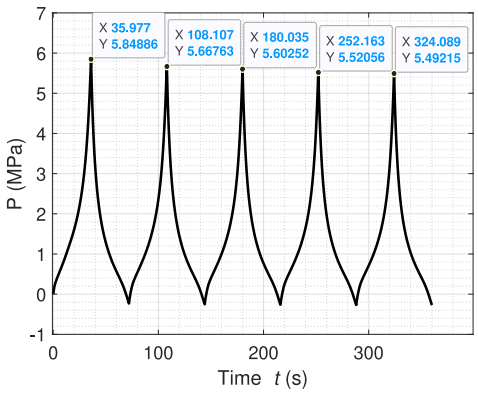

Fig. 13. The stress values at the peaks for the following cycles of compression of syntactic foam $\phi = 40\%$ with the strain 50% as in Fig. 11(c).

measured response of syntactic foams at small strain, and this also differs in tension and due to the means of sample attachment (glued or otherwise) [22,67]. What is perhaps important here however is the order of magnitude of Young's modulus, which is similar to that determined in [6]. Given the nonlinear fit across a large time domain in this case, it is perhaps inevitable that the linear modulus is not necessarily precisely consistent with a linear mechanics analysis based on micromechanics, which would yield an increasing modulus as a function of volume fraction. An alternative approach would be to use micromechanics to fix the Young's modulus at a specific volume fraction for each syntactic foam sample, checking that this is consistent with the experimental determination of the modulus at small volume fraction. This could then be employed as a fixed parameter in the QLV model, as per the Poisson ratio Hencky model, permitting a further reduction in the number of parameters and hence reducing computational costs further. This is an aspect of research that will be considered in future studies, but is beyond the scope of the present work.

6.5. Viscoelastic properties of syntactic foams

The time-dependent relaxation functions depicted in Fig. 15 display the viscoelastic properties of unfilled PU and syntactic foam with filling fractions of 20% and 40%. The results are shown by using only the OgII model with $N = 2$, being overall one of the most accurate as previously demonstrated (although in some cases OgI can perform even better, see for example Section 6.1 for further details). Unfilled PU exhibits low dissipation during the one loading–unloading cycle since insignificant decay of long time shear and bulk modulus, as reflected by $\mu_\infty/\mu = 0.9690$ and $\kappa_\infty/\kappa = 0.9465$. This is consistent with the experiments as shown in Fig. 6(c-d) where hysteresis effects are negligible. In contrast, the addition of microsphere hollow particles to the PU matrix enhances non-negligible dissipation and time-sensitive behaviour, as evidenced by $\mu_\infty/\mu = 0.9507$ and $\kappa_\infty/\kappa = 0.0890$ for the 20% and $\mu_\infty/\mu = 0.7532$ and $\kappa_\infty/\kappa = 0.2001$ for the 40% filling fraction consistently to experimental curves shown in Figs. 7(c–d) and 8(c–d), respectively. This suggests that the hollow space inside the microsphere particles serves as miniature dampers, effectively absorbing energy. More energy is required to deform the tiny shell of the microsphere particles during the loading than is required to release it to its initial shape (assuming it fully recovers).

7. Concluding remarks

We have developed a quasi-linear viscoelastic model for polymer-based syntactic foams under cyclic compression, enabling the determination of their natural material properties and perhaps more importantly, understood the nature of the general fitting strategy across a range of strains. The experimental data obtained for various filling fractions demonstrates the compressibility, recoverability, and energy dissipation of these materials. By utilising multiple strain energy functions and the Prony series, we were able to estimate the viscoelastic material properties and SEF coefficients through optimisation curve fitting. We have considered SF 20% and 40% in the analysis, and we plan to investigate the more challenging SF 50% in the future.

Our results indicate that the modelling of unfilled PU is straightforward due to its simple behaviour and microstructure. The Ogden type-I SEF is the most effective and provides the best fitting. In contrast, the CnH SEF is more suitable for unfilled PU rather than SFs. Additionally, the fitted model for lower strain is not suitable for larger strain fitting. Furthermore, we discovered that the fitting model acquired from the first cyclic period is applicable to all cyclic processes, providing a more efficient approach for future studies. Overall, this research provides valuable insights into the behaviour of polymer-based syntactic foams under cyclic compression, with applications in various engineering fields. Various factors can contribute to the intricate mechanical response of SFs under compression. The negative stress observed during experiments when the glued sample returns to its original position, the noticeable hysteresis effects, and the numerous recent studies cited in the literature all point towards the use of nonlinear viscoelasticity in an attempt to explain the complex behaviours of SFs under compression. We demonstrated here that QLV is an approach that has merit in describing the response of such materials under large deformation.

Finally, our study reveals that the addition of microsphere hollow particles to the PU matrix results in more viscoelastic and time-sensitive syntactic foams. These materials exhibit unique characteristics, such as reduced stiffness and increased energy dissipation, which make them suitable for various applications, such as impact protection and damping systems. Our findings contribute to a better understanding of the mechanical behaviour of syntactic foams and can help to optimise their use in different engineering fields. Understanding how to tailor the material nonlinearity associated with specific distributions of shell radii and shell thickness has future potential in a wide range of applications.

CRediT authorship contribution statement

Sy-Ngoc Nguyen: Writing – review & editing, Writing – original draft, Validation, Software, Methodology, Investigation, Formal analysis, Data curation, Conceptualization. **Riccardo De Pascalis:** Writing – review & editing, Writing – original draft, Visualization, Validation, Supervision, Methodology, Investigation, Formal analysis, Conceptualization. **Zeshan Yousaf:** Writing – review & editing, Writing – original draft, Visualization, Validation, Methodology, Investigation, Data curation, Conceptualization. **William J. Parnell:** Writing – review & editing, Visualization, Validation, Supervision, Resources, Project administration, Methodology, Investigation, Funding acquisition, Formal analysis, Conceptualization.

Declaration of competing interest

The authors declare that they have no known competing financial interests or personal relationships that could have appeared to influence the work reported in this paper.

Acknowledgements

S-NN, ZY, WJP are grateful to the Engineering and Physical Sciences Research Council (EPSRC) for funding via grant EP/S019804/1. RDP's work is carried out under the auspices and the partial support of GNFM (Gruppo Nazionale di Fisica Matematica) of Italian INdAM and the support of 'Progetto Tisma', CUP F83C21000150001 PNR–MUR, M4C2–Dalla ricerca all'impresa—1.1: Fondo per il Programma Nazionale della Ricerca (PNR) e Progetti di Ricerca di Rilevante Interesse Nazionale (PRIN).

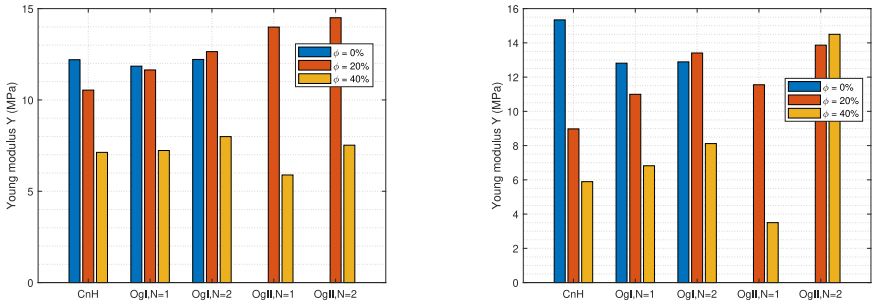

(a) 25% compression (b) 50% compression

Fig. 14. Young modulus Y estimation. (For interpretation of the references to colour in this figure legend, the reader is referred to the web version of this article.)

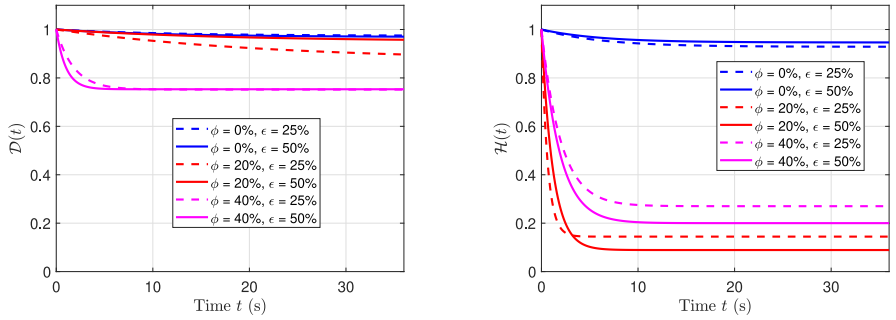

(a) The scalar relaxation function $\mathcal{D}(t)$. (b) The scalar relaxation function $\mathcal{H}(t)$.

Fig. 15. The time-dependent reduced-relaxation functions for shear and bulk modulus. (For interpretation of the references to colour in this figure legend, the reader is referred to the web version of this article.)

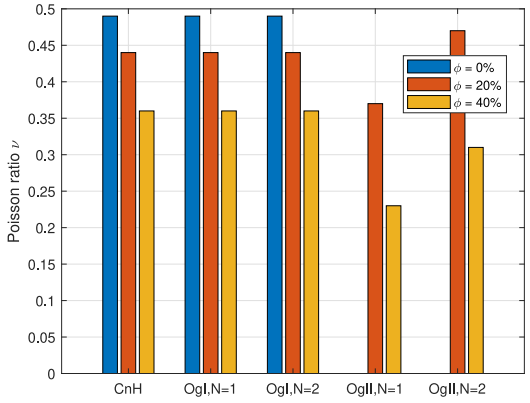

Fig. 16. Poisson ratio ν estimation from previous work [6]. (For interpretation of the references to colour in this figure legend, the reader is referred to the web version of this article.)

Appendix A. Poisson ratio

See Fig. 16.

Appendix B. RMSE values

See Tables 2–6.

Appendix C. Supplementary data

Supplementary material related to this article can be found online at https://doi.org/10.1016/j.compositesb.2024.111866.

Table 2
The RMSE values for compression strains up to 25%.

RMSE - 25% of strain compression					
ϕ	CnH	OgI		OgII	
		$N = 1$	$N = 2$	$N = 1$	$N = 2$
0	0.0142	0.0075	0.0142	–	–
20%	0.1028	0.0873	0.0553	0.1424	0.0472
40%	0.1026	0.0891	0.0586	0.1321	0.1028

Table 3
The RMSE values for compression strains up to 50%.

RMSE - 50% of strain compression					
ϕ	CnH	OgI		OgII	
		$N = 1$	$N = 2$	$N = 1$	$N = 2$
0	0.5500	0.0205	0.0278	–	–
20%	0.5016	0.1202	0.0938	0.3170	0.2763
40%	0.2058	0.1170	0.0786	0.1739	0.1806

Table 4
Testing the 25% fitted model for the 50% experiment data.

RMSE - 25% over 50%					
ϕ	CnH	OgI		OgII	
		$N = 1$	$N = 2$	$N = 1$	$N = 2$
0	0.5622	0.4715	0.6646	–	–
20%	0.6439	0.4129	6.8430	0.8698	5.9673
40%	0.2208	0.1852	7.3791	0.2696	0.7646

Table 5
Testing the 50% fitted model for the lower strain 25% experiment data.

RMSE - 50% over 25%					
ϕ	CnH	OgI		OgII	
		$N = 1$	$N = 2$	$N = 1$	$N = 2$
0	0.1237	0.0179	0.0193	–	–
20%	0.2200	0.1632	0.1179	0.1136	0.1147
40%	0.1239	0.1190	0.0886	0.1595	0.1512

Table 6
Testing the one cycle fitted models over all five cycles.

RMSE - across 5 cycles					
ϕ	CnH	OgI		OgII	
		$N = 1$	$N = 2$	$N = 1$	$N = 2$
0	0.5065	0.1064	0.1105	–	–
40%	0.3094	0.2624	0.2357	0.2788	0.2898

Data availability

Experimental data are provided as supporting material. The values computed from the optimisation process are detailed in the Supplementary Material files.

References

[1] Gupta N, Zeltmann SE, Shunmugasamy VC, Pinisetty D. Applications of polymer matrix syntactic foams. Jom 2014;66(2):245–54.
[2] Afolabi LO, Ariff ZM, Hashim SFS, Alomayri T, Mahzan S, Kamarudin K-A, Muhammad ID. Syntactic foams formulations, production techniques, and industry applications: A review. J Mater Res Technol 2020;9(5):10698–718.
[3] Wu X, Gao Y, Wang Y, Fan R, Ali Z, Yu J, Yang K, Sun K, Li X, Lei Y, et al. Recent developments on epoxy-based syntactic foams for deep sea exploration. J Mater Sci 2021;56:2037–76.
[4] Lu X, Li Y, Chen Z, Li S, Wang X, Liu Q. Recent trends in polymer matrix solid buoyancy materials: A review. Polymers 2024;16(16). http://dx.doi.org/10.3390/polym16162307, URL https://www.mdpi.com/2073-4360/16/16/2307.
[5] Yousaf Z, Smith M, Potluri P, Parnell W. Compression properties of polymeric syntactic foam composites under cyclic loading. Composites B 2020;186:107764.
[6] Smith MJ, Yousaf Z, Potluri P, Parnell WJ. Modelling hollow thermoplastic syntactic foams under high-strain compressive loading. Compos Sci Technol 2021;213:108882.
[7] Curd ME, Morrison NF, Smith MJ, Gajjar P, Yousaf Z, Parnell WJ. Geometrical and mechanical characterisation of hollow thermoplastic microspheres for syntactic foam applications. Composites B 2021;223:108952.
[8] Gupta N. A functionally graded syntactic foam material for high energy absorption under compression. Mater Lett 2007;61(4–5):979–82.
[9] Arencon D, Velasco J, Realinho V, Sanchez-Soto M, Gordillo A. Fracture toughness of glass microsphere-filled polypropylene and polypropylene/poly (ethylene terephthalate-co-isophthalate) blend-matrix composites. J Mater Sci 2007;42:19–29.
[10] Rabiei A, O'Neill A. A study on processing of a composite metal foam via casting. Mater Sci Eng A 2005;404(1):159–64. http://dx.doi.org/10.1016/j.msea.2005.05.089, URL https://www.sciencedirect.com/science/article/pii/S0921509305005332.
[11] Weise J, Zanetti-Bueckmann V, Yezerska O, Schneider M, Haesche M. Processing, properties and coating of micro-porous syntactic foams. Adv Energy Mater 2007;9(1–2):52–6. http://dx.doi.org/10.1002/adem.200600198, arXiv: https://onlinelibrary.wiley.com/doi/pdf/10.1002/adem.200600198 URL https://onlinelibrary.wiley.com/doi/abs/10.1002/adem.200600198.
[12] Linul E, Lell D, Movahedi N, Codrean C, Fiedler T. Compressive properties of zinc syntactic foams at elevated temperatures. Composites B 2019;167:122–34.
[13] Kemény A, Movahedi N, Fiedler T, Maróti JE, Orbulov IN. The influence of infiltration casting technique on properties of metal syntactic foams and their foam-filled tube structures. Mater Sci Eng A 2022;852:143706. http://dx.doi.org/10.1016/j.msea.2022.143706, URL https://www.sciencedirect.com/science/article/pii/S0921509322010905.
[14] Maróti JE, Orbulov IN. Characteristic compressive properties of AlSi7Mg matrix syntactic foams reinforced by Al2O3 or SiC particles in the matrix. Mater Sci Eng A 2023;869:144817. http://dx.doi.org/10.1016/j.msea.2023.144817, URL https://www.sciencedirect.com/science/article/pii/S0921509323002411.
[15] Prabhakar P, Feng H, Subramaniyan SP, Doddamani M. Densification mechanics of polymeric syntactic foams. Composites B 2022;232:109597.
[16] Bunn P, Mottram J. Manufacture and compression properties of syntactic foams. Composites 1993;24(7):565–71.
[17] Huang J, Gibson L. Elastic moduli of a composite of hollow spheres in a matrix. J Mech Phys Solids 1993;41(1):55–75.
[18] Kochetkov V. Calculation of deformative and thermal properties of multiphase composite materials filled with composite or hollow spherical inclusions by the effective medium method. Mech Compos Mater 1996;31(4):337–45.
[19] d'Almeida J. An analysis of the effect of the diameters of glass microspheres on the mechanical behavior of glass-microsphere/epoxy-matrix composites. Compos Sci Technol 1999;59(14):2087–91.
[20] Bardella L, Genna F. On the elastic behavior of syntactic foams. Int J Solids Struct 2001;38(40–41):7235–60.
[21] Gupta N, Woldesenbet E. Microballoon wall thickness effects on properties of syntactic foams. J Cell Plast 2004;40(6):461–80.
[22] Yousaf Z, Morrison NF, Parnell WJ. Tensile properties of all-polymeric syntactic foam composites: experimental characterization and mathematical modelling. Composites B 2022;231:109556.
[23] Carolan D, Mayall A, Dear J, Fergusson A. Micromechanical modelling of syntactic foam. Composites B 2020;183:107701.
[24] Jones GW, Smith MJ, Thorpe M, Abrahams ID, Parnell WJ. Transition from equatorial to whole-shell buckling in embedded spherical shells under axisymmetric far-field loading. Int J Solids Struct 2022;256:111957.
[25] Paget B, Zinet M, Cassagnau P. Syntactic foam under compressive stress: Comparison of modeling predictions and experimental measurements. J Cell Plast 2021;57(3):329–46.
[26] Kim HS, Plubrai P. Manufacturing and failure mechanisms of syntactic foam under compression. Composites A 2004;35(9):1009–15.
[27] De Pascalis R, David Abrahams I, Parnell WJ. Predicting the pressure–volume curve of an elastic microsphere composite. J Mech Phys Solids 2013;61(4):1106–23. http://dx.doi.org/10.1016/j.jmps.2012.11.005, URL https://www.sciencedirect.com/science/article/pii/S0022509612002438.
[28] Huang R, Li P. Elastic behaviour and failure mechanism in epoxy syntactic foams: The effect of glass microballoon volume fractions. Composites B 2015;78:401–8.
[29] Shrimali B, Parnell WJ, Lopez-Pamies O. A simple explicit model constructed from a homogenization solution for the large-strain mechanical response of elastomeric syntactic foams. Int J Non-Linear Mech 2020;126:103548.
[30] Lawrence E, Pyrz R. Viscoelastic properties of polyethylene syntactic foam with polymer microballoons. Polym Polym Compos 2001;9(4):227–37.
[31] Poveda RL, Achar S, Gupta N. Viscoelastic properties of carbon nanofiber reinforced multiscale syntactic foam. Composites B 2014;58:208–16.
[32] Gupta N, Shunmugasamy VC. High strain rate compressive response of syntactic foams: Trends in mechanical properties and failure mechanisms. Mater Sci Eng A 2011;528(25–26):7596–605.
[33] Hariharan G, Khare D, Upadhyaya P. A micromechanical model to predict the viscoelastic response of syntactic foams. Mater Today: Proc 2020;28:1200–4.
[34] Subramaniyan SP, Prabhakar P. Moisture-driven degradation mechanisms in the viscoelastic properties of TPU-Based syntactic foams. Polym Degrad Stab 2023;218:110547.
[35] Bardella L, Genna F, et al. Some remarks on the micromechanical modeling of glass/epoxy syntactic foams. In: Proceedings of 20th annual technical conference of the American society for composites. DEStech Publications Lancaster, PA, USA; 2005, p. 1–21.
[36] Capela C, Ferreira JAM, Costa JDM. Viscoelastic properties assessment of syntactic foams by dynamic mechanical analysis. In: Materials science forum. Vol. 636, Trans Tech Publ; 2010, p. 280–6.
[37] Xu T, Li G. Cyclic stress-strain behavior of shape memory polymer based syntactic foam programmed by 2-D stress condition. Polymer 2011;52(20):4571–80. http://dx.doi.org/10.1016/j.polymer.2011.08.005, URL https://www.sciencedirect.com/science/article/pii/S0032386111006537.
[38] Hariharan G, Khare D, Upadhyaya P. A micromechanical model to predict the viscoelastic response of syntactic foams. Mater Today: Proc 2020;28:1200–4. http://dx.doi.org/10.1016/j.matpr.2020.01.216, URL https://www.sciencedirect.com/science/article/pii/S2214785320302820 2nd International Conference on Recent Advances in Materials & Manufacturing Technologies.
[39] Christensen RM. Theory of viscoelasticity. Courier Corporation; 2003.
[40] Wineman AS, Rajagopal KR. Mechanical response of polymers: an introduction. Cambridge University Press; 2000.
[41] Papanicolaou G, Zaoutsos S. Viscoelastic constitutive modeling of creep and stress relaxation in polymers and polymer matrix composites. In: Creep and fatigue in polymer matrix composites. Elsevier; 2019, p. 3–59.
[42] Nguyen S-N, Lee J, Cho M. Efficient higher-order zig-zag theory for viscoelastic laminated composite plates. Int J Solids Struct 2015;62:174–85.
[43] Brown TS, Du S, Eruslu H, Sayas F-J. Analysis of models for viscoelastic wave propagation. Appl Math Nonlinear Sci 2018;3(1):55–96.
[44] Nguyen S-N, Lee J, Han J-W, Cho M. A coupled hygrothermo-mechanical viscoelastic analysis of multilayered composite plates for long-term creep behaviors. Compos Struct 2020;242:112030.
[45] Nguyen S-N, Cho M, Kim J-S, Han J-W. Improved thermo-mechanical-viscoelastic analysis of laminated composite structures via the enhanced Lo–Christensen–Wu theory in the laplace domain. Mech Adv Mater Struct 2023;30(14):2899–915.

[46] Wineman A. Nonlinear viscoelastic solids—A review. Math Mech Solids 2009;14(3):300–66. http://dx.doi.org/10.1177/1081286509103660, arXiv:https://doi.org/10.1177/1081286509103660.

[47] Fung YC. Biomechanics, 2nd ed.. New York: Springer-Verlag; 1993, http://dx.doi.org/10.1007/978-1-4757-2257-4.

[48] De Pascalis R, Abrahams ID, Parnell WJ. On nonlinear viscoelastic deformations: a reappraisal of Fung's quasi-linear viscoelastic model. Proc R Soc A 2014;470(2166):20140058.

[49] Berjamin H, Destrade M, Parnell WJ. On the thermodynamic consistency of quasi-linear viscoelastic models for soft solids. Mech Res Commun 2021;111:103648.

[50] Balbi V, Shearer T, Parnell WJ. Tensor decomposition for modified quasi-linear viscoelastic models: Towards a fully non-linear theory. Math Mech Solids 2024;29(6):1064–88. http://dx.doi.org/10.1177/10812865231165232, arXiv:https://doi.org/10.1177/10812865231165232.

[51] Rajagopal K, Wineman A. A quasi-correspondence principle for quasi-linear viscoelastic solids. Mech Time-Dependent Mater 2008;12:1–14.

[52] Sarver JJ, Robinson PS, Elliott DM. Methods for quasi-linear viscoelastic modeling of soft tissue: application to incremental stress-relaxation experiments. J Biomech Eng 2003;125(5):754–8.

[53] De Pascalis R, Abrahams ID, Parnell WJ. Simple shear of a compressible quasilinear viscoelastic material. Internat J Engrg Sci 2015;88:64–72. http://dx.doi.org/10.1016/j.ijengsci.2014.11.011, URL https://www.sciencedirect.com/science/article/pii/S0020722514002353, Special Issue on "Qualitative Methods in Engineering Science".

[54] Selyutina N, Argatov I, Mishuris G. On application of Fung's quasi-linear viscoelastic model to modeling of impact experiment for articular cartilage. Mech Res Commun 2015;67:24–30.

[55] Babaei B, Velasquez-Mao AJ, Thomopoulos S, Elson EL, Abramowitch SD, Genin GM. Discrete quasi-linear viscoelastic damping analysis of connective tissues, and the biomechanics of stretching. J Mech Behav Biomed Mater 2017;69:193–202.

[56] De Pascalis R, Parnell WJ, Abrahams ID, Shearer T, Daly DM, Grundy D. The inflation of viscoelastic balloons and hollow viscera. Proc R Soc A 2018;474(2218):20180102. http://dx.doi.org/10.1098/rspa.2018.0102, arXiv:https://royalsocietypublishing.org/doi/pdf/10.1098/rspa.2018.0102 URL https://royalsocietypublishing.org/doi/abs/10.1098/rspa.2018.0102.

[57] Helisaz H, Bacca M, Chiao M. Quasi-linear viscoelastic characterization of soft tissue-mimicking materials. J Biomech Eng 2021;143(6):061007. http://dx.doi.org/10.1115/1.4050036, arXiv:https://asmedigitalcollection.asme.org/biomechanical/article-pdf/143/6/061007/6664051/bio_143_06_061007.pdf.

[58] Aryeetey OJ, Frank M, Lorenz A, Estermann S-J, Reisinger AG, Pahr DH. A parameter reduced adaptive quasi-linear viscoelastic model for soft biological tissue in uniaxial tension. J Mech Behav Biomed Mater 2022;126:104999. http://dx.doi.org/10.1016/j.jmbbm.2021.104999, URL https://www.sciencedirect.com/science/article/pii/S1751616121006251.

[59] Giudici A, van der Laan KW, van der Bruggen MM, Parikh S, Berends E, Foulquier S, Delhaas T, Reesink KD, Spronck B. Constituent-based quasi-linear viscoelasticity: a revised quasi-linear modelling framework to capture nonlinear viscoelasticity in arteries. Biomech Model Mechanobiol 2023;1–17.

[60] Helisaz H, Belanger E, Black P, Bacca M, Chiao M. Quantifying the impact of cancer on the viscoelastic properties of the prostate gland using a quasi-linear viscoelastic model. Acta Biomater 2024;173:184–98. http://dx.doi.org/10.1016/j.actbio.2023.11.002, URL https://www.sciencedirect.com/science/article/pii/S1742706123006487.

[61] Parnell WJ, De Pascalis R. Soft metamaterials with dynamic viscoelastic functionality tuned by pre-deformation. Phil Trans R Soc A 2019;377(2144):20180072. http://dx.doi.org/10.1098/rsta.2018.0072, arXiv:https://royalsocietypublishing.org/doi/pdf/10.1098/rsta.2018.0072 URL https://royalsocietypublishing.org/doi/abs/10.1098/rsta.2018.0072.

[62] Berjamin H, De Pascalis R. Acoustoelastic analysis of soft viscoelastic solids with application to pre-stressed phononic crystals. Int J Solids Struct 2022;241:111529. http://dx.doi.org/10.1016/j.ijsolstr.2022.111529, URL https://www.sciencedirect.com/science/article/pii/S0020768322000828.

[63] De Pascalis R, Napoli G, Saccomandi G. Kink-type solitary waves within the quasi-linear viscoelastic model. Wave Motion 2019;86:195–202. http://dx.doi.org/10.1016/j.wavemoti.2018.12.004, URL https://www.sciencedirect.com/science/article/pii/S0165212518303950.

[64] Dadgar-Rad F, Firouzi N. Time-dependent response of incompressible membranes based on quasi-linear viscoelasticity theory. Int J Appl Mech 2021;13(03):2150036. http://dx.doi.org/10.1142/S1758825121500368, arXiv:https://doi.org/10.1142/S1758825121500368.

[65] Dadgar-Rad F, Firouzi N. Large deformation analysis of two-dimensional visco-hyperelastic beams and frames. Arch Appl Mech 2021;91:4279–301.

[66] Firouzi N, Rabczuk T, Bonet J, Żur KK. A computational framework for large strain electromechanics of electro-visco-hyperelastic beams. Comput Methods Appl Mech Engrg 2024;426:116985. http://dx.doi.org/10.1016/j.cma.2024.116985, URL https://www.sciencedirect.com/science/article/pii/S004578252400241X.

[67] Fatt MSH, Chen L. A viscoelastic damage model for hysteresis in PVC H100 foam under cyclic loading. J Cell Plast 2015;51(3):269–87. http://dx.doi.org/10.1177/0021955X14537659, arXiv:https://doi.org/10.1177/0021955X14537659.

[68] Wouterson EM, Boey FY, Hu X, Wong S-C. Specific properties and fracture toughness of syntactic foam: Effect of foam microstructures. Compos Sci Technol 2005;65(11):1840–50. http://dx.doi.org/10.1016/j.compscitech.2005.03.012, URL https://www.sciencedirect.com/science/article/pii/S0266353805000837.

[69] Rickaby S, Scott N. A cyclic stress softening model for the Mullins effect. Int J Solids Struct 2013;50(1):111–20.

[70] Mihai LA, Goriely A. How to characterize a nonlinear elastic material? A review on nonlinear constitutive parameters in isotropic finite elasticity. Proc R Soc A 2017;473(2207):20170607. http://dx.doi.org/10.1098/rspa.2017.0607, arXiv:https://royalsocietypublishing.org/doi/pdf/10.1098/rspa.2017.0607 URL https://royalsocietypublishing.org/doi/abs/10.1098/rspa.2017.0607.

[71] Jridi N, Arfaoui M, Hamdi A, Salvia M, Bareille O, Ichchou M, Ben Abdallah J. Separable finite viscoelasticity: integral-based models vs. experiments. Mech. Time-Depend. Mater. 2019;23(3):295–325. http://dx.doi.org/10.1007/s11043-018-9383-2.

[72] Wang LM, Linka K, Kuhl E. Automated model discovery for muscle using constitutive recurrent neural networks. J Mech Behav Biomed Mater 2023;145:106021. http://dx.doi.org/10.1016/j.jmbbm.2023.106021, URL https://www.sciencedirect.com/science/article/pii/S1751616123003740.

[73] Balbi V, Shearer T, Parnell WJ. A modified formulation of quasi-linear viscoelasticity for transversely isotropic materials under finite deformation. Proceedings of the Royal Society A: Mathematical, Physical and Engineering Sciences 2018;474(2217):20180231. http://dx.doi.org/10.1098/rspa.2018.0231, arXiv:https://royalsocietypublishing.org/doi/pdf/10.1098/rspa.2018.0231 URL https://royalsocietypublishing.org/doi/abs/10.1098/rspa.2018.0231.

[74] Ogden RW. Non-linear elastic deformations. New York: Dover; 1997, Reprint of Ellis Harwood Ltd, Chichester, (1984).

[75] Berezvai S, Kossa A. Closed-form solution of the Ogden–Hill's compressible hyperelastic model for ramp loading. Mech Time-Dependent Mater 2017;21:263–86.

[76] Yan S, Jia D, Yu Y, Wang L, Qiu Y, Wan Q. Novel strategies for parameter fitting procedure of the Ogden hyperfoam model under shear condition. Eur J Mech A Solids 2021;86:104154. http://dx.doi.org/10.1016/j.euromechsol.2020.104154, URL https://www.sciencedirect.com/science/article/pii/S0997753820305374.

[77] Ogden RW. Recent advances in the phenomenological theory of rubber elasticity. Rubber Chem Technol 1986;59(3):361–83. http://dx.doi.org/10.5254/1.3538206, arXiv:https://meridian.allenpress.com/rct/article-pdf/59/3/361/1937858/1_3538206.pdf.

[78] Ali A, Hosseini M, Sahari BB. A review of constitutive models for rubber-like materials. Am J Eng Appl Sci 2010;3:232–9, URL https://api.semanticscholar.org/CorpusID:33961726.

[79] Ogden RW, Hill R. Large deformation isotropic elasticity – on the correlation of theory and experiment for incompressible rubberlike solids. Proc R Soc A 1972;326(1567):565–84. http://dx.doi.org/10.1098/rspa.1972.0026, arXiv:https://royalsocietypublishing.org/doi/pdf/10.1098/rspa.1972.0026 URL https://royalsocietypublishing.org/doi/abs/10.1098/rspa.1972.0026.

[80] Hill R. Aspects of invariance in solid mechanics. In: Yih C-S, editor. Advances in applied mechanics - book series. Vol. 18, Elsevier; 1979, p. 1–75. http://dx.doi.org/10.1016/S0065-2156(08)70264-3, URL https://www.sciencedirect.com/science/article/pii/S0065215608702643.

[81] Storåkers B. On material representation and constitutive branching in finite compressible elasticity. J Mech Phys Solids 1986;34(2):125–45. http://dx.doi.org/10.1016/0022-5096(86)90033-5, URL https://www.sciencedirect.com/science/article/pii/0022509686900335.

[82] Ogden RW, Saccomandi G, Sgura I. Fitting hyperelastic models to experimental data. Comput Mech 2004;34:484–502.

[83] Gutmann H-M. A radial basis function method for global optimization. J Glob Optim 2001;19(3):201–27.

[84] Viana FA, Haftka RT, Watson LT. Efficient global optimization algorithm assisted by multiple surrogate techniques. J Global Optim 2013;56:669–89.

[85] Shorter R, Thomas AG, Busfield JJC, Smith JD. The physical behaviour of elastomers containing hollow spherical fillers. In: Boukamel A, Laiarinandrasana L, Meo S, Verron E, editors. Constitutive models for rubber v: proceedings of the 5th European conference, Paris, France, 4-7 September 2007. London: Taylor and Francis; 2008, p. 107–12.

[86] Paget B, Zinet M, Cassagnau P. Syntactic foam under compressive stress: Comparison of modeling predictions and experimental measurements. J Cell Plast 2021;57(3):329–46. http://dx.doi.org/10.1177/0021955X20943112, arXiv:https://doi.org/10.1177/0021955X20943112.